JMEPEG (2011) 20:1285–1288
DOI: 10.1007/s11665-010-9747-5

1059-9495/$19.00

Cyclic Oxidation Behavior of Simulated Post-Weld Heat-Treated P91

S. Rajendran Pillai and R.K. Dayal

(Submitted December 4, 2009; in revised form July 8, 2010)

For long-term service life it is desirable that the high-temperature components posses slow-growing oxide scale. The growth and degradation of the oxide scale on P91 were studied by a thermal cycling method. The oxidation temperature was 780 °C and the duration of each cycle was 2 h. The mass gain and integrity of the scale was examined using a thermogravimetric balance. Any lack of integrity is monitored by the transient mass gain associated with the exposure of fresh surface. The scale retained the integrity throughout 100 cycles. Post-oxidation examination was carried out by scanning electron microscopy, energy dispersive spectroscopy and laser Raman spectroscopy. The nature of the scale was characterized and the reason for the compositional segregation is analyzed.

Keywords carbon/alloy steels, chemical analysis, corrosion testing, energy, metallography

1. Introduction

High-temperature components in energy systems require predictable and economically viable life times in the system. It is also necessary to keep the thickness of the components to an optimum level to facilitate good mass transfer and moderate the cost of construction material. Fast breeder reactors employ steels of different grades for the various components. In the construction of steam generator, the prime concern is the compatibility with high-temperature steam. Ferritic steels of the modified 9Cr-1Mo grade (commercially called P91) finds wide spread applications in engineering systems. This choice is based on the good mechanical properties coupled with excellent resistance to aqueous corrosion. This alloy is employed in the fabrication of steam generator and decay heat removal systems of fast reactors. Yet another important property of the material is the integrity of the oxide scale (Ref 1-4). An adherent oxide scale enables low wastage of material during high-temperature service. The factors limiting the integrity of the oxide scale have been reviewed and reported in the literature (Ref 5-7). The present investigation is aimed at understanding the oxidation behavior of P91 after subjecting to post-weld heat treatment. The experiment was carried out in the cyclic mode as it was evident that more than the high temperature it is the cycling between two temperatures that affects the integrity of the scale (Ref 1, 8).

S. Rajendran Pillai and **R.K. Dayal**, Corrosion Science and Technology Division, Indira Gandhi Centre for Atomic Research, Kalpakkam 603102 Tamil Nadu, India. Contact e-mail: essarpe12@yahoo.co.in.

2. Experimental

The material selected for oxidation studies was P91 of composition given in Table 1.

The material was heat-treated under the following conditions: 1050 °C for 30 min and tempered at 760 °C for 3 h. This procedure is imparted to simulate the post-weld heat treatments normally given to large components after fabrication. A specimen of size 20 × 10 × 3 mm was cut from this material. It was then polished to 5 μm surface finish using successive grades of polishing paper. The polished specimen was washed with tap water then with soap water. It was cleaned ultrasonically with acetone. The average grain size was 25 μm.

Thermogravimetry (Setsys-12, Setaram, France) was employed in the present investigation. The thermogravimetric balance has a measuring sensitivity of 0.1 μg. The integrity of the oxide scale was monitored by "Transient mass gain" method, developed in this laboratory (Ref 1). This method monitors the mass changes accompanying the oxidation in a real-time mode. Any accelerated rate of oxidation due to failure in integrity of the scale and exposure of fresh surface is indicated by an abrupt increase in the mass for a short period. The data is continuously acquired using software called SETSOFT. The experimental conditions are depicted in Fig. 1.

- Temperature of oxidation: 780 °C
- Heating rate (AB and EF): 30 °C/min
- Cooling rate (CD and GH): 20 °C/min
- Retention time (BC and FG): 2 h for each cycle
- Retention time between cycles (DE): 1 h

Oxidation kinetics was obtained in the form of mass gain measurements. After completing the 100 cycles (200 h of oxidation) the specimen was examined by employing laser Raman spectrophotometer (LRS), scanning electron microscope (SEM), and energy dispersive spectroscopy (EDS) for the analysis of oxide scales which are formed on the surface of the specimen. Raman experiment was carried out with an HR 800 (Jobin Yvon) Raman spectrometer equipped with 1800

Table 1 Chemical composition of modified 9Cr-1Mo material

Elements	Mass %
C	0.1
Cr	9.5
Mo	1.0
Si	0.48
Mn	0.39
V	0.25
Nb	0.1
S	0.009
P	0.021
Ni	0.14
Al	0.024
N	0.0650
Fe	Balance

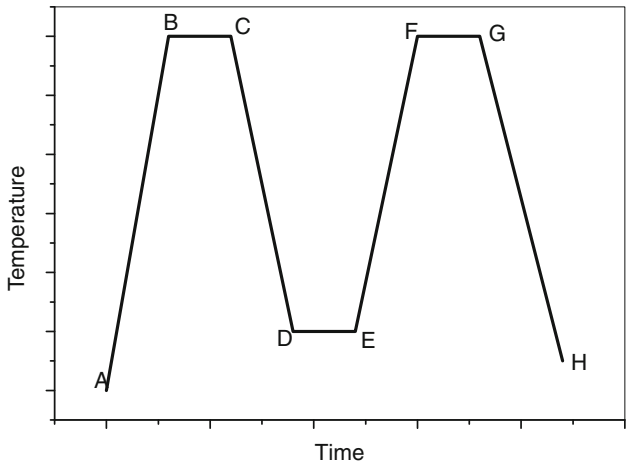

Fig. 1 Schematic representation of conditions of the thermogravimetric measurement

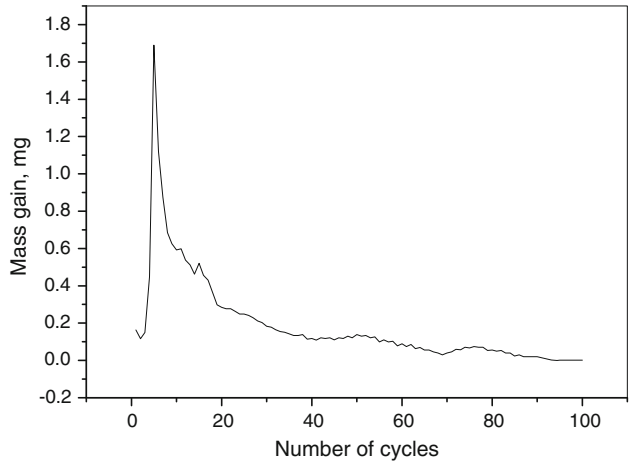

Fig. 2 Data of mass gain in each cycle

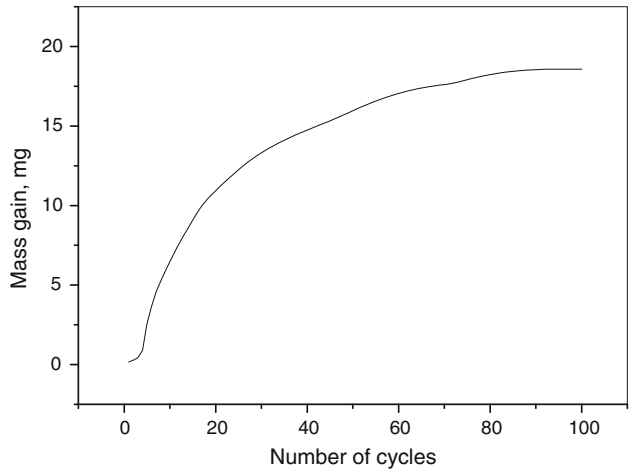

Fig. 3 Data of cumulative mass gain

grooves/mm holographic grating. Argon laser of 488 nm was used as an excitation source. The laser spot size focused on the surface was approximately 2 μm and laser power was 10 mW at the sample. Both Raman excitation and emission were performed using a 10× long distance objective with 180° back scattering.

3. Results and Discussion

The results of mass gain obtained in each cycle are shown in Fig. 2. The mass gain was initially higher, reaching a maximum in the fifth cycle. Thereafter the mass gain progressively decreased and reached a steady value after 20 cycles. The initial high rate of oxidation is attributed to the exposure of fresh surface when the oxidation proceeds by a linear kinetics. The mass gain follows a combination of linear and parabolic rate law up to 20 cycles. Thereafter the scale already formed dictates a parabolic rate. The cumulative mass gain data shown in the Fig. 3 show a parabolic behavior. In ferrous alloys, the diffusion of cation from the bulk matrix to reach the surface to react with oxygen is the rate-limiting step. This diffusional mode of oxidation results in a parabolic rate law.

Thermogravimetric analysis did not show any failure in integrity of the scale. There was no spallation during the full course of the investigation. The scale was adherent or it has not attained the critical thickness to attain spallation. The mass gain revealed increasing rates in the initial cycle and attained a maximum in the fifth cycle. This is due to the exposure of freshly polished surface and the contribution of linear rate to the overall oxidation. As the scale thickens the oxidation is more controlled by diffusion and a parabolic rate is established. This is reflected in the reduced mass gain in the successive cycles. As the thickness of the pre-existing layer increases the mass gain in each cycle is progressively reduced.

The morphology of the surface was analyzed using scanning electron microscopy (SEM) and the features corresponding to different magnifications are shown in Fig. 4(a) to (d).

Figure 4(a) shows the features of a generally adherent scale free from cracks and of spalled region. It shows that the surface has several undulations and indicates the presence of oxide nodules. The oxide nodules are generated by faster rate of diffusion through short circuit diffusion paths (Ref 9, 10).

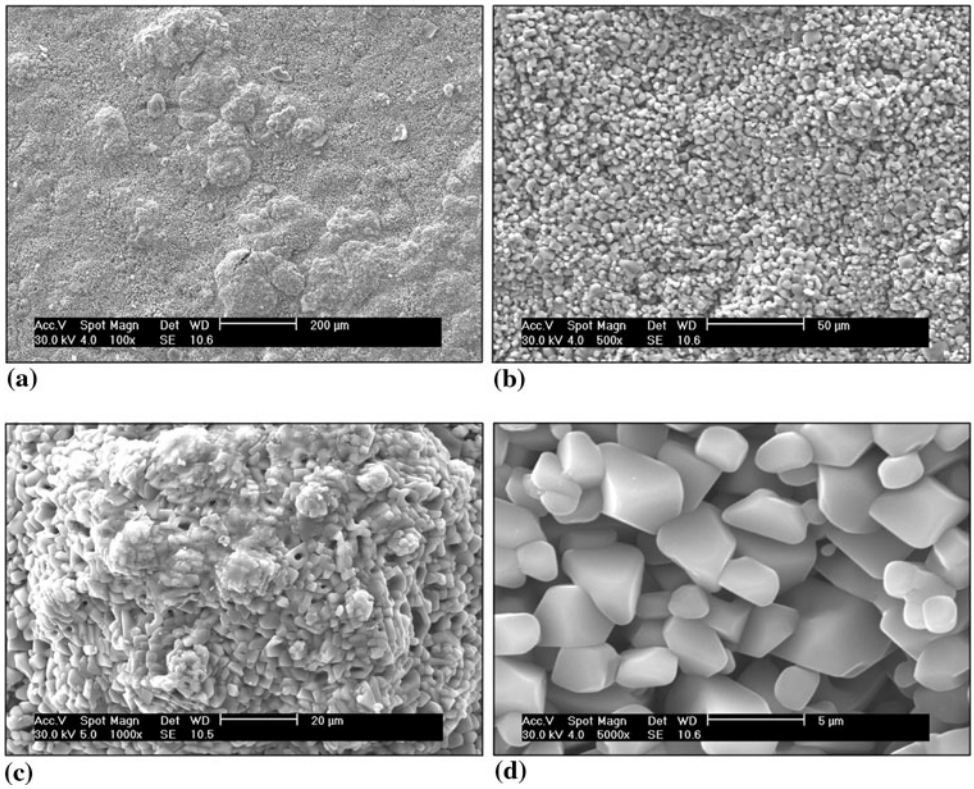

Fig. 4 Overall surface view showing nodules on the surface (a) and fine precipitates of oxides (b), (c) view showing porous outgrowth, (d) magnified view of crystalline oxides

Table 2 Composition of different regions by EDS analysis

Region	Composition/mass %
Overall uniform area	Si = 1.04 Cr = 4.63 Fe = 94.33
Adherent oxide scale	Si = 1.95 Cr = 3.63 Fe = 94.42
Porous out growth of small area	Si = 1.83 Cr = 6.40 Fe = 91.77
Porous outgrowth of larger area	Si = LD Cr = 8.98 Fe = 91.02

LD, less than detection limit

These paths are perceived to be grain boundaries. In grain boundary regions, chromium diffuses faster and thus promotes its enhanced rate to reach the surface. It is also possible that the analyzing beam has penetrated the bulk which indicated a higher chromium concentration. Further experiments are required to fully understand the reason for high concentration of chromium. Figure 4(b) shows the features of an outgrowth. There was enhancement in the concentration of chromium at this region pointing to the enhanced diffusion of chromium through the short circuit diffusion paths. Figure 4(c) and (d) shows the crystalline nature of the oxide scale. The scale has not showed any sintering characteristics, but remained adherent.

The diffusion of iron through the pre-existing oxide scale is an order of magnitude faster than that of chromium. Thus, even though chromium oxide is thermodynamically more stable, chromium diffuses slower than iron. Thus surface region is covered by a layer of iron oxide. However, iron oxide is less adherent. Thus, high-temperature oxidation leads to the

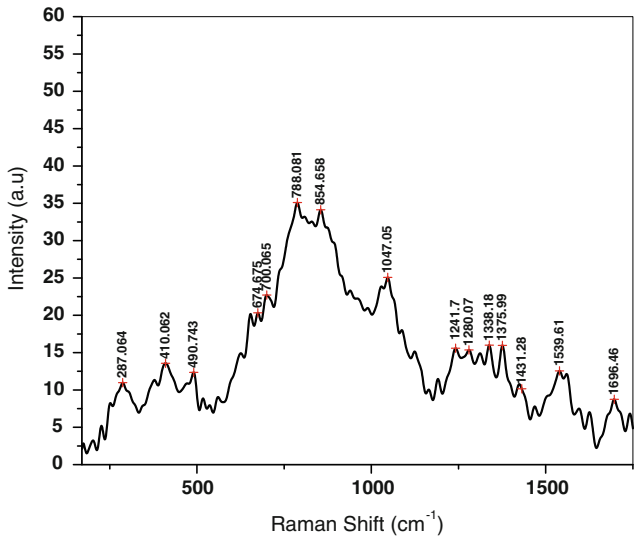

Fig. 5 Raman spectroscopic analysis of the oxidized surface

generation of less stable and less adherent iron oxide at the surface (Ref 1). However, in the present conditions of investigation, the scale remained adherent.

This analytical results obtained by energy dispersive spectroscopy (EDS) are shown in Table 2.

The nodular region showed enhancement in the concentration of chromium compared to the flat region.

The results of analysis by laser Raman spectroscopy (LRS) of the oxide surface are shown in Fig. 5.

Table 3 Raman frequency assignments for various oxides on the P 91 alloy

Band, cm^{-1}	Assignments	Band, cm^{-1}	Assignments
287	Iron oxide phases	788, 800-950	Mixed oxides of iron and chromium
380, 410, 490	Iron and chromium (III) oxides	1000-1047	Mixed oxides of vanadium and molybdenum
520, 560	Chromium (III) oxides	1124, 1190	Oxides of iron
636, 650-700	Iron oxides, spinel	Other small peaks	Un assigned

It was observed from the Raman spectra that the heated surface of the alloy consists of mixed oxides of iron chromium, molybdenum. Also the presence of vanadium was sensed. Overall, the obtained Raman spectrum was broad and consists of overlapping of various spectral signatures due to the oxides of iron, chromium, molybdenum, and vanadium. In this regard, it is really difficult to confirm the presence of oxide scales of one particular element based on Raman experiments alone. Because, the oxides of molybdenum and vanadium and some phases of iron and chromium fall in the same frequency region and hence the tentative frequency assignments have been made.

Table 3 shows the Raman spectral analysis of the oxide scale of the oxidized specimen. The tentative peak assignments have been made based on literature findings (Ref 11-14).

4. Conclusion

Cyclic oxidation studies on the coarse grain region of P91 (simulated weld) was carried out at 780 °C. The duration of each cycle was 2 h and we have carried out 100 cycles. The study revealed that

i. The integrity of the scale was maintained throughout the cycles it was free from cracks and buckling. There was no evidence of spallation either
ii. SEM investigation revealed that the surface is not uniform but contains intermittent nodules. This nodular out growth was the result of oxidation of cation diffusing through short circuit diffusion paths such as grain boundaries
iii. Analysis of EDS revealed that the nodular regions are enriched in chromium. The rate of diffusion of iron through the pre-existing scale is faster than that of chromium. But in the short circuit diffusion paths, chromium also diffuses fast, and being thermodynamically more stable than iron oxide, preferentially forms oxide on the surface
iv. Analysis by laser Raman spectroscopy supported the above data. This method could also identify the existence of minor oxides like that of vanadium and molybdenum. Analysis by Raman spectroscopy is only indicative of the phases and not confirmative. EDS analysis gives the relative composition of metals and silicon ignoring the content of oxygen. The result is thus approximate, but indicates the correct trend.

Acknowledgments

The authors wish to acknowledge the sincere co-operation of Mrs. M. Radhika in carrying out the SEM and EDS analyses and S. Ramya in the Raman spectroscopic analysis.

References

1. S. Rajendran Pillai and R.K. Dayal, Cyclic Oxidation of P91 by Thermogravimetry and Investigation of the Integrity of the Scale by Transient Mass Gain Method, *Oxid. Met.*, 2008, **69**(3–4), p 131–142
2. S. Rajendran Pillai, P. Shankar, and H.S. Khatak, Cyclic Oxidation of P91 at 1073, 1123 and 1173 K, *High Temp. Mater. Process.*, 2004, **23**(3), p 196–204
3. M. Schuetze, Deformation and Cracking Behaviour of Protective Oxide Scale on Heat-Resistant Steels Under Tensile Strain, *Oxid. Met.*, 1985, **24**(3/4), p 199–232
4. S. Rajendran Pillai, Life History of Oxide Scales in Metals and Alloys, *Corros. Rev.*, 2005, **23**(4–6), p 277–328
5. W.J. Quadakkers and K. Bongartz, The Prediction of Breakaway Oxidation for Alumina Forming ODS Alloys Using Oxidation Diagram, *Werkst. Korros.*, 1994, **45**, p 232–241
6. M. Schuetze, Plasticity of Protective Oxide Scale, *Mater. Sci. Technol.*, 1990, **6**, p 32–38
7. R. Hales, The High Temperature Oxidation Behaviour of Austenitic Stainless Steel, *Werkst. Korros.*, 1978, **29**, p 393–399
8. D. Monceau and D. Poquillon, Continuous Thermogravimetry Under Cyclic Conditions, *Oxid. Met.*, 2004, **61**(1/2), p 143–153
9. R. Peraldi and B. Pint, Effect of Cr and Ni Contents on the Oxidation Behaviour of Ferritic and Austenitic Model Alloys in Air with Water Vapour, *Oxid. Met.*, 2004, **61**, p 463–483
10. S. Jianian, Z. Longjiang, and L. Tiefan, High Temperature Oxidation of Fe-Cr Alloy in Wet Oxygen, *Oxid. Met.*, 1997, **48**(3/4), p 347–356
11. D. Jeremy Ramsaey, L. Richard, and L. McCreery, Raman Microscopy of Chromate Interactions with Corroding Aluminum Alloy 2024–T3, *Corros. Sci.*, 2004, **46**, p 1729–1739
12. D.S. Dunn, M.B. Bogart, C.S. Brossiand, and G.A. Cragnolino, Corrosion of Iron Under Alternate Wet and Dry Conditions, *Corrosion*, 2000, **56**, p 470–488
13. X.J. Wang, H.D. Li, Y.J. Fei, X. Wang, Y.Y. Xiong, Y.X. Nie, and K.A. Feng, XRD and Raman Studies of Vanadium Oxide Thin Films Deposited on Fused Silica Substrate by RF Magnetron Sputtering, *Appl. Surf. Sci.*, 2001, **177**, p 8–14
14. T. Onfroy, O.V. Manoilova, S.B. Nukallah, D.M. Hercules, G. Clet, and M. Haoullah, Surface Structure and Catalytic Performance of Niobium Oxide Supported on Titania, *Appl. Catal. A*, 2007, **316**, p 184–190